Soft Matter

PAPER

View Article Online
View Journal | View Issue

Motion transition of active filaments: rotation without hydrodynamic interactions

Cite this: *Soft Matter*, 2014, **10**, 1012

Huijun Jiang and Zhonghuai Hou*

We investigate the dynamics of an active semiflexible filament in a bead–rod model involving dynamically the hydrodynamic interaction (HI), active force, filament flexibility and viscous drag. We find that the filament can show three distinct types of motion, namely, translation, snaking and rotation, with the variation of the rigidity or active force. The transition from translation to snaking is continuous and mainly due to transverse instability, while the snaking–rotation transition is first-order like and shown to result from a type of symmetry breaking associated with the shape kinematics. Of particular interest, we find that HI is not necessary for the rotation or snaking motion, but can enlarge remarkably the parameter regions in which they can occur. Combining with local collisions, we show that, for the parameter region where HI is essential for the maintenance of rotation curvature of a single filament, HI is also essential for the emergence of collective vortexes. Thus, our findings provide new insights into the subtle role of HI in the formation of collective structures in active systems.

Received 30th August 2013
Accepted 26th November 2013

DOI: 10.1039/c3sm52291a

www.rsc.org/softmatter

1 Introduction

Collective behaviors emerging spontaneously in active systems, ranging from flocks of birds and schools of fish to self-propelled catalytic nanoparticles and microorganisms, have attracted rapidly increasing attention. In this regard, motility assays where semiflexible filaments are driven to slide over a bed of myosin molecular motors now receive great research interest due to their easy implement *in vitro* and sufficient parameter control.[1–5]

Several recent experiments have revealed that active filaments can self-organize into fascinating coherently moving structures, such as propagating density waves and vortexes.[1,2] Interestingly, conflicting viewpoints about the formation mechanism of vortexes have been drawn by two similar motility assay experiments. The collective motion of actin filaments driven by meromyosin was studied by Volker Schaller *et al.*[1] The authors believed that the hydrodynamic interaction (HI) is essential for the formation of vortexes by comparing collective motions in experiments with those in cellular automata simulations. In contrast, Yutaka Sumino *et al.* investigated the vortex formation of microtubules driven by dynein c,[2] wherein the authors argued that HI is not necessary for the formation of vortexes. By the analysis of the motion of a single filament and collisions between filaments in very low filament density, they believed that the intrinsic property of a single microtubule to maintain the smoothness and curvature of its rotation trajectory, combined with aligning interactions induced by the local collision of microtubules, is the very reason for the vortex formation. In addition, they also pointed out that such a persistence of smooth rotation motion is the consequence of that each single filament has a relatively large number (about 100) of motors attached on it, and thus is driven by a large active force.

These two experiments present a very attractive topic on how a collective vortex structure emerges, especially what is the real role of HI in the formation process. It is noted that the emergence of collective vortexes is a multiscale process, involving the motion of a single filament with intra-filament interactions and the collective movement of multi-filaments with inter-filament interactions. HI may affect self-organization of vortexes at different scales, for example, the maintenance of rotation curvature at the single-filament scale, filament–filament interactions at the multi-filament scale, or even interactions between clusters of filaments. As a first step towards the theoretical study of the formation mechanism of vortexes, a thorough investigation of the motion of a single active filament is required to provide insights for the maintenance of rotation curvature and to understand the role of HI at the single-filament level.

In this paper, we investigate the movement of a single active filament based on a simple theoretical model involving the HI, active force, filament flexibility, and viscous drag dynamically. We find that the filament can show three distinct types of spontaneous motion, namely, translation (T), snaking (S) and rotation (R): as the rigidity (denoted by the parameter κ) decreases, the filament undergoes a transition from T to S at $\kappa = \kappa_1$ and then to R at $\kappa \leq \kappa_2$. We show that the T–S transition at

Department of Chemical Physics & Hefei National Laboratory for Physical Sciences at Microscales, University of Science and Technology of China, Hefei, Anhui 230026, China. E-mail: hzhlj@ustc.edu.cn

κ_1 is due to the instability of transverse movement, and the S–R transition at κ_2 results from symmetry breaking associated with the shape kinematics. Scaling analysis near κ_1 and a qualitative linear stability analysis of the translation suggest a continuous transition *via* a supercritical bifurcation, while a bistable character in the vicinity of κ_2 indicates a first-order-like transition. Similar motion transitions are also found as the active force increases. Of particular interest, we find that rotation can be observed without HI, but the parameter region for its appearance is significantly enlarged if HI takes effect. Consequently, a filament driven by larger force is more likely to show rotation, while HI can help one driven by smaller force to rotate. Furthermore, collective behaviors are directly investigated by considering only intra-filament HI and local collisions of filaments. For filaments driven by small forces, vortexes emerge only if HI is taken into account. These findings thus provide a possible explanation at the single-filament level for the controversial points proposed above and also new insights into the subtle role of HI in active systems.

2 Model and method

Usually, the dynamics of the active filament is governed by low Reynolds number hydrodynamics, where viscous effects dominate and inertial effects are negligible.[6] It involves the active driving by motor proteins walking on the filament, which convert chemical energy into work and generate active force. So far, several theoretical models have been proposed to describe the active filament, which may be grouped into two main types. In models of the first type, the filament is described by using a continuum elasticity approximation, which allows an elegant theoretical analysis of its shape kinematics.[7–10] Interestingly, depending on different end boundary conditions, motions such as filament undulation (buckling) or rotation are found.[9,10] For other types of models, one mainly focuses on the effects of HI, but with simple well-controlled shape kinematics[4] or (partially) fixed filament shapes.[11] These models either neglect the shape kinematics of each filament segment, which should arise spontaneously by the interaction between the driving, filament flexibility, and viscous drag,[12] or miss the HI effect, both of which should be considered to study the spontaneous motion of a filament, especially the effect of HI on it.

In our study, the filament is modeled as a chain of N beads with positions $\mathbf{r}_i$ connected by $N-1$ rigid rods as shown in Fig. 1, interacting through a potential given by

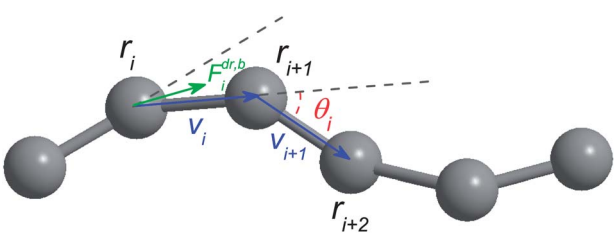

Fig. 1 Bead-rod model of the active filament.

$$U(\mathbf{r}_1,\cdots,\mathbf{r}_N)=\sum_{i=1}^{N-2}U^{\mathrm{B}}(\mathbf{v}_i,\mathbf{v}_{i+1})+\frac{1}{2}\sum_{i,j=1;j\neq i}^{N}U^{\mathrm{LJ}}(\mathbf{r}_i-\mathbf{r}_j), \quad (1)$$

which will lead to a force $-\partial U/\partial \mathbf{r}_i$ to the ith bead. Herein, the three-body bending potential $U^{\mathrm{B}}(\mathbf{v}_i,\mathbf{v}_{i+1})=\frac{1}{2}\left(\frac{\kappa}{\pi}\right)\theta_i^2$, with bond vectors $\mathbf{v}_i=\mathbf{r}_{i+1}-\mathbf{r}_i$ and κ to measure the filament rigidity, tends to keep the angle θ_i between $\mathbf{v}_i$ and $\mathbf{v}_{i+1}$ close to its equilibrium value of zero. The Lennard-Jones repulsive potential $U^{\mathrm{LJ}}(\mathbf{r}_i-\mathbf{r}_j)=4\xi\left\{\left(\frac{2a}{r_{ij}}\right)^{12}-\left(\frac{2a}{r_{ij}}\right)^{6}\right\}+\xi$, which exists only if the distance between beads $r_{ij}=|\mathbf{r}_i-\mathbf{r}_j|$ is less than $2\sqrt[6]{2}a$ (a is the bead radius), accounts for the exclusive volume effects. Besides the potential U, the bead positions are constrained by the rigid rods which are assumed to be inextensible. Such rigid constraints are realized in the present work by the so-called FENE-Fraenkel (FF) spring with the force given by[13]

$$\mathbf{F}^{\mathrm{sp}}(\mathbf{v})=\frac{H(|\mathbf{v}|-v_0)}{1-(|\mathbf{v}|-v_0)^2/(v_0\delta)^2}\frac{\mathbf{v}}{|\mathbf{v}|},\ \text{for}\ (1-\delta)<\frac{|\mathbf{v}|}{v_0}<(1+\delta), \quad (2)$$

where H (usually very large) is the spring constant and δ is the extensibility parameter that defines the maximum possible departure of the spring length from its natural value v_0. The use of this particular type of spring avoids the complexity introduced by other algorithms like SHAKE-HI[14] and facilitates the use of a relatively large simulation time step. Consequently, the force that is exerted by the FF-springs on bead i is given by $\mathbf{F}_i^{\mathrm{sp,b}}=\mathbf{F}^{\mathrm{sp}}(\mathbf{v}_i)-\mathbf{F}^{\mathrm{sp}}(\mathbf{v}_{i-1})$.

In experiments, the filaments are driven by molecular motors binding to them. The motors slide along a filament and propel it to the opposite direction. Detailed models taking into account explicitly the number and positions of motors have been proposed to study the motion of rod-like filaments.[4] In the stationary state, the active force nearly balances the friction force, leading to a nearly constant speed as also observed in experiments. Assuming homogeneous distribution of motors on the surface, it is reasonable to suggest that the active force on the unit length of the filament can be viewed as a constant. Using this approximation, we assume that each bond $\mathbf{v}_j$ is subject to a constant force α along its direction, *i.e.*, $\mathbf{F}^{\mathrm{dr}}(\mathbf{v}_j)=\alpha\hat{\mathbf{v}}_j$ with $\hat{\mathbf{v}}_j=\mathbf{v}_j/|\mathbf{v}_j|$. Accordingly, the active force on bead i is then $\mathbf{F}_i^{\mathrm{dr,b}}=\mathbf{F}^{\mathrm{dr}}(\mathbf{v}_i)+\mathbf{F}^{\mathrm{dr}}(\mathbf{v}_{i-1})$.

Taking into account the interaction potential, bond constraints and active driven forces given above, the time evolution of the bead positions $\mathbf{r}_i(t)$ is then governed by the following over-damped Langevin equation with HI included,

$$\dot{\mathbf{r}}_i(t)=\sum_{j=1}^{N}\mu_{ij}(\mathbf{r}_{ij})\left[-\frac{\partial U(\mathbf{r}_1,\cdots,\mathbf{r}_N)}{\partial \mathbf{r}_j}+\mathbf{F}_j^{\mathrm{sp,b}}+\mathbf{F}_j^{\mathrm{dr,b}}\right]+\varsigma_i(t). \quad (3)$$

Herein, HI between two different beads i and j is implemented *via* the Ronte–Prager–Yamakawa mobility tensor[15,16]

$$\mu_{ij}=\mu_0\left[\frac{3}{4}ar_{ij}^{-1}(1+\hat{\mathbf{r}}_{ij}\hat{\mathbf{r}}_{ij})+\frac{1}{2}a^3r_{ij}^{-3}(1-3\hat{\mathbf{r}}_{ij}\hat{\mathbf{r}}_{ij})\right],(i\neq j,\ \ r\geq 2a) \quad (4a)$$

$$\mu_{ij} = \mu_0 \left[\left(1 - \frac{9}{32}\frac{r_{ij}}{a} \right) \mathbf{1} + \frac{3}{32}\frac{r_{ij}\hat{\mathbf{r}}_{ij}\hat{\mathbf{r}}_{ij}}{a} \right]. \quad (i \neq j, \;\; r \leq 2a) \qquad (4b)$$

The self-mobility of bead i is given by $\mu_{ii} = \mu_0\mathbf{1}$ with $\mu_0 = 1/(6\pi\eta a)$ and η being the viscosity of the aqueous solvent. $\mathbf{1}$ denotes the three-dimensional unit matrix and $\hat{\mathbf{r}}_{ij}\hat{\mathbf{r}}_{ij}$ is the outer product of the normalized vectors $\hat{\mathbf{r}}_{ij} = \mathbf{r}_{ij}/r_{ij}$. $\zeta(t)$ models the random force from the heat bath and obeys the fluctuation–dissipation theorem $\langle \zeta_i(t)\zeta_j(t')\rangle = 2k_BT_0\mu_{ij}\delta(t-t')$ with k_B being the Boltzmann constant and T_0 being the temperature. Since the filament is fixed on a plane, in simulations, we set the z-axis of Cartesian coordinates to be perpendicular to the plane at $z = 0$, *i.e.*, all the positions of the beads are $\mathbf{r} = (x, y, 0)$. Since the filament is fixed in a plane, forces along the z-axis are always considered to be in equilibrium. Thus, the model we proposed describes a two-dimensional dynamics with three-dimensional hydrodynamics. We discretize eqn (3) with time step Δ, and an implicit predictor–corrector method is employed to realize the rod-length constraint as described in detail in ref. 13. The noise terms are numerically implemented by using Cholesky decomposition. We rescale the length, time and energy by $2a$, Δ and ξ, respectively, and thus the dimensionless self-mobility is $\tilde{\mu}_0 = \mu_0\xi\Delta/(2a)^2$. In experiments, stable directed movement of active filaments is observed, implying that the time scale for rotational diffusion of the rodlike filament is much larger than the one for a clear observation of the filament motion. In simulations, similar time-scale separation can be observed by taking $k_BT_0 = \xi/100$. Other parameters are $v_0/(2a) = 2$, $N = 10$ (thus $L/(2a) = 18$) and $\alpha/10^3 = 4$ if not otherwise stated. All the output results are generated by simulations for total time steps $T_{tot} > 10^7$.

3 Results

Firstly, we are interested in how the filament motion depends on the flexibility for a fixed active force. Typically, three types of motion are observed in different parameter regions of κ as outlined in Fig. 2(a). When the filament is rigid enough, say $\kappa > \kappa_1$, both the shape and trajectory of the filament are straight lines. This translation motion (T) loses its stability for $\kappa < \kappa_1$, where the filament snakes along a straight direction. With further decreasing κ, the snaking motion (S) suddenly becomes unstable at a certain κ_2, where the filament starts to rotate around a circle (rotation motion, R). To characterize these three distinct modes of motion, we introduce an order parameter Q as follows:

$$Q = \frac{1}{C_0 T_{tot}} \left| \int_0^{T_{tot}} \dot{\mathbf{R}}_{CM} \mathrm{d}t \right|, \qquad (5)$$

where $\dot{\mathbf{R}}_{CM}$ denotes the center-of-mass velocity of the filament, T_{tot} is the total simulation time, and C_0 is the speed of the translation motion. According to this definition, Q equals to 1 for translation, 0 for the rotation, and a value in between for snaking. Q as a function of κ is also shown in Fig. 2(a), where two transition points at $\kappa_1/10^3 \simeq 6.0$ and $\kappa_2/10^3 \simeq 1.9$ are clearly presented. The T–S transition at κ_1 looks continuous, while the S–R transition at κ_2 is more likely to be of first-order

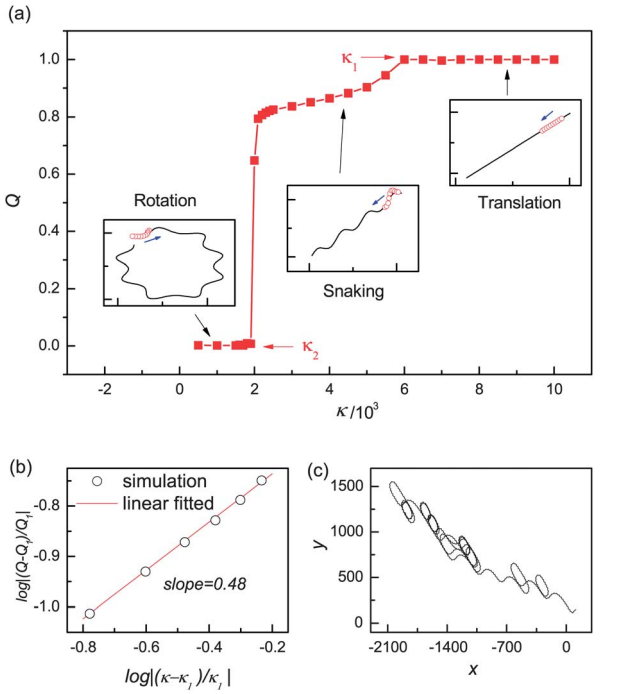

Fig. 2 (a) Order parameter Q (time-average velocity of the center-of-mass) as a function of rigidity κ, showing transition between three types of filament motion. Insets: typical trajectories for translation ($\kappa/10^3 = 8$), snaking ($\kappa/10^3 = 4$) and rotation ($\kappa/10^3 = 1.5$). (b) Scaling behavior near the translation–snaking transition point κ_1. The simulation result can be well fitted by a line with slope 0.48 (c) mixed-type of active filament motion observed near the snaking–rotation transition point κ_2.

(discontinuous). To check the former, we have performed scaling analysis near κ_1. As shown in Fig. 2(b), the dependence of $\log|(Q - Q_1)/Q_1|$ on $\log|(\kappa - \kappa_1)/\kappa_1|$, where Q_1 is the value of Q at κ_1, can be well fitted by a line with slope 0.48. This implies that the snaking motion may arise from instability of translation *via* a supercritical bifurcation.[9] In close vicinity of κ_2, however, we observed a mixed type of motion as shown in Fig. 2(c). The filament seems to jump randomly from snaking to rotation and back to snaking repeatedly. This observation suggests a bistable nature near κ_2, which supports the existence of a first-order like transition there.

To elucidate the underlying mechanisms of these two transitions, we have investigated how the shape kinematics changes for different types of motion, which is represented by the departure of the moving direction of an individual bead (for example, the first bead) from that of the center-of-mass. Clearly, for translation, the angle φ between $\dot{\mathbf{r}}_1$ and $\dot{\mathbf{R}}_{CM}$ is nearly zero, and so are the angles θ_i (the angle between the adjacent bonds $\mathbf{v}_i$ and $\mathbf{v}_{i+1}$) shown in Fig. 1. We thus may investigate the stability of the T-motion against the active force and the flexibility, by accounting for the dynamics of θ_i. To this end, we take the three adjacent beads shown in Fig. 1 for a simple qualitative illustration. Ignoring the HI, the force that tends to enlarge θ_i results from the active driving acting on the center bead (the $i + 1$ bead) and is proportional to $\alpha \sin \theta_i$, while that tends to reduce θ_i is given by the bending force applied on the side bead (the $i + 2$

bead) and reads $\kappa\theta_i/\pi$. Approximately, one may write $\dot{\theta}_i \propto \alpha \sin \theta_i - \kappa\theta_i/\pi$. It is easy to check that the solution $\theta_i = 0$ of this equation, corresponding to the T-motion, loses its linear stability when $\kappa \leq \alpha\pi$. This may provide a reasonable explanation for the transition at κ_1, though the exact value does not coincide. For the S-motion, the angles θ_i and also φ should not be zero anymore, and it is hard to write simple dynamic equations for them. Numerically, we find that φ shows a symmetric bimodal distribution with two sharp peaks at relatively large deviations from zero, as demonstrated in Fig. 3(a). The distance between the two peaks increases continuously from 0 (the vertical line) with decreasing κ from κ_1, in agreement with the continuous transition features. For $\kappa \leq \kappa_2$, however, this symmetric distribution of φ is broken as shown in Fig. 3(c). Apparently, the angle φ gets biased to more negative values here (for clockwise rotation) for smaller κ. This particular symmetry breaking regarding the shape kinematics of the filament is in coincidence with a first-order like transition at κ_2. A theoretical model that analytically accounts for this symmetry-breaking transition should certainly help, however, it is not available at the present stage and also beyond the main scope of the present study.

The above studies evidently show that rotation can be a spontaneous motion for a single flexible filament. Nevertheless, all the results so far are obtained from the simulation of eqn (3), where HI has already been explicitly considered. In a recent paper,[5] although using a different model, the authors emphasized that HI is essential for an active filament to rotate. It is therefore rather interesting for us to investigate the very role of HI in the occurrence of rotation, as well as the transition behaviors shown in Fig. 2. Note that in our simulation, HI can be conveniently turned off by setting all the off-diagonal elements of the mobility tensor to be zero, *i.e.*, $\mu_{ij} = 0$ for $i \neq j$ in eqn (3). Interestingly, the three types of filament motion and motion transitions can also be found even if the HI is excluded. The distributions of the angle φ for filament motions without HI are also presented in Fig. 3(b) and (d). A similar symmetric bimodal distribution with two sharp peaks is found for the S-motion, and a symmetric-broken distribution in which the angle φ prefers more positive values (for anticlockwise rotation) appears for the R-motion. These findings indicate that the filament motion transitions originate from the same underlying mechanisms no matter HI is present or not.

In order to understand the similarity of transitions with and without HI as well as the role played by the friction, we now look back at the over-damped dynamical equation eqn (3). It can be found that the friction (*i.e.*, the mobility tensor in the over-damped dynamics) takes effect as a coefficient matrix. For the non-HI case, the coefficients of the beads are the same unit matrix, while they are different when HI is present. Again, taking the three adjacent beads in Fig. 1 as an example, the forces that affect the change of the angle are the active force acting on the center bead and the bending force acting on the side bead. Hence, the HI induced differences of the coefficient matrix can lead to effective forces larger or smaller than the corresponding real ones. According to the aforementioned instability analysis, this will result in a change of the transition boundary (which will be validated in what follows) but not the underlying mechanism.

We have performed extensive simulations to get the phase diagram of the filament motion with HI in the α–κ plane as shown in Fig. 4(a). With increasing activity α, both κ_1 (T–S boundary) and κ_2 (S–R boundary) increase linearly. This indicates that a larger active force is required for a less-flexible filament to snake or rotate, which sounds reasonable because a

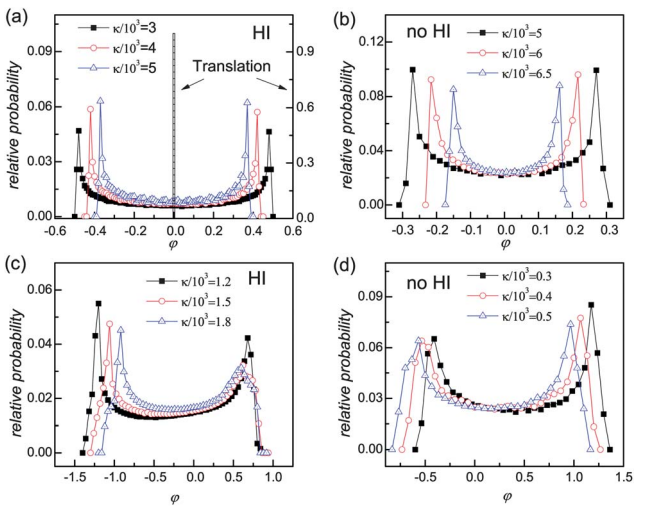

Fig. 3 Distribution of the angle φ between moving direction of the first bead and that of the center-of-mass, for snaking (a and b) and rotation ((c) for clockwise and (d) for anticlockwise)). Results with HI are shown in (a) and (c), while those without HI are in (b) and (d). The active force without HI is set to be $\alpha/10^3 = 12$. The vertical bar in (a) shows the distribution of φ for translation.

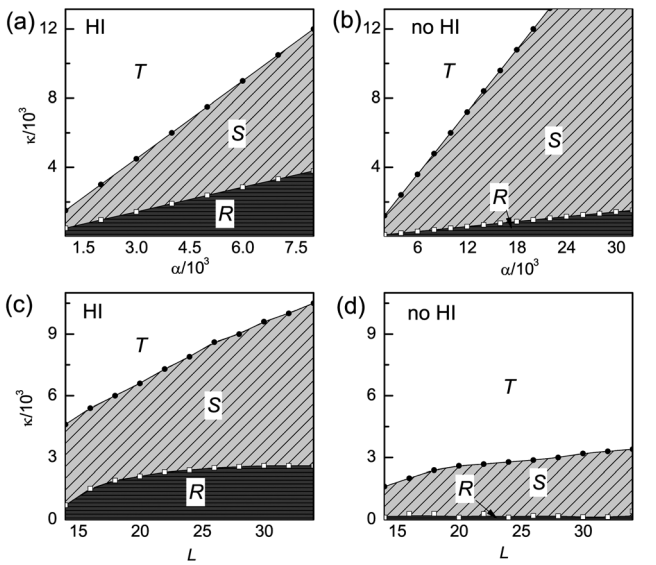

Fig. 4 Phase diagrams of filament motion. Parameters α, κ and L represent the active force, filament rigidity and filament length, respectively. Results with HI are shown in (a) and (c), while those without HI are in (b) and (d). T, S, and R stand for translation, snaking, and rotation, respectively. $L = 18$ in (a) and (b) and $\alpha/10^3 = 4$ in (c) and (d). Note that the range of α in (b) is much larger than in (a).

rigid filament tends to move straightly and a strong active force may lead to its transverse instability in a friction environment. The linear dependence between κ_1 and α agrees with the simple analysis described in the last paragraph, while the reasoning behind that regarding κ_2 and α remains open. In Fig. 4(b), the phase diagram similar to that in Fig. 4(a), but without HI, is presented. Importantly, we find that the rotation motion can still be observed, but the parameter range for it (dark region) is much smaller compared to that in Fig. 4(a). This demonstrates that HI is not necessary for the rotation of a filament, but rather can enhance considerably the parameter region for observing it. We have also investigated how the filament motion depends on its length L. The phase diagrams in the $L-\kappa$ plane for fixed $\alpha = 4$ are shown in Fig. 4(c) and (d), with and without HI, respectively. Clearly, the T–S and S–R transition behaviors are robust to the filament length. Again, the parameter regions for snaking and rotation are considerably enlarged when HI is present.

4 Discussion

To figure out whether the intra-filament HI effects on single filament motion are sufficient to provide possible understanding of the controversial points proposed in the beginning of the paper, we now investigate the emergence of collective structures from many filaments by assuming the same local collisions as in ref. 2. There, the authors observed aligning interactions between colliding filaments, and thus they established a theoretical model with such local collisions to investigate the collective behaviors. Here, a similar many-filament model is proposed to describe the dynamics of M interacting filaments, in which rotating filaments are represented by identical point particles moving in rotation at constant speed C_0, and interact as follows,

$$\frac{d\mathbf{q}_i}{dt} = C_0\left(\mathbf{e}_x\cos\Theta_i + \mathbf{e}_y\sin\Theta_i\right) \tag{6a}$$

$$\frac{d\Theta_i}{dt} = \omega_i + \beta\sum\sin\left(2\left(\Theta_j - \Theta_i\right)\right) + \xi(t), \tag{6b}$$

where $\mathbf{q}_i$, Θ_i and ω_i are the position, orientation and intrinsic angular velocity of particle i, respectively. $\mathbf{e}_x$ and $\mathbf{e}_y$ are unit vectors in the x and y directions. $\xi(t)$ is a Gaussian white noise with zero mean and variance σ^2 to present possible fluctuations of the angular velocity. The sum in eqn (6b) is over all particles within the interaction distance of particle i (which is naturally chosen to be the filament length L as in ref. 2), and β is the interaction strength. In the many-filament model, the dynamic parameters of the single-filament model will take effect by affecting ω_i which the filament rotates at in the many-filament model. Without losing generality, all simulations are started with random initial conditions and C_0 is set to be unity. The simulation area is $64L \times 64L$. Periodic boundary conditions are used. As mentioned in ref. 2 and as observed in simulations, collective vortexes only arise for relatively high densities. Thus, we fix $M = 320$ and $\beta = 0.1$ if not otherwise stated.

Collective behaviors in the parameter region where the intra-filament HI is important for the appearance of single filament rotation (for example, active force $\alpha/10^3 = 6$, filament rigidity $\kappa/10^3 = 1.3$ and filament length $L = 18$) are shown in Fig. 5. When intra-filament HI takes effect, a particle rotates with $\omega_i \sim 0.2$ (which results in a rotation curvature whose size is approximately equal to the one of a single-filament rotation with the given parameters), and σ^2 is taken to be 0.02 to estimate roughly the variance. It can be observed that collective vortexes emerge spontaneously and develop stably from interacting filaments. For the same parameters without HI (filaments move along a straight line, and $\omega_i = 0$), directed propagations of filaments are formed instead of vortexes. Comparison between Fig. 5(a) and

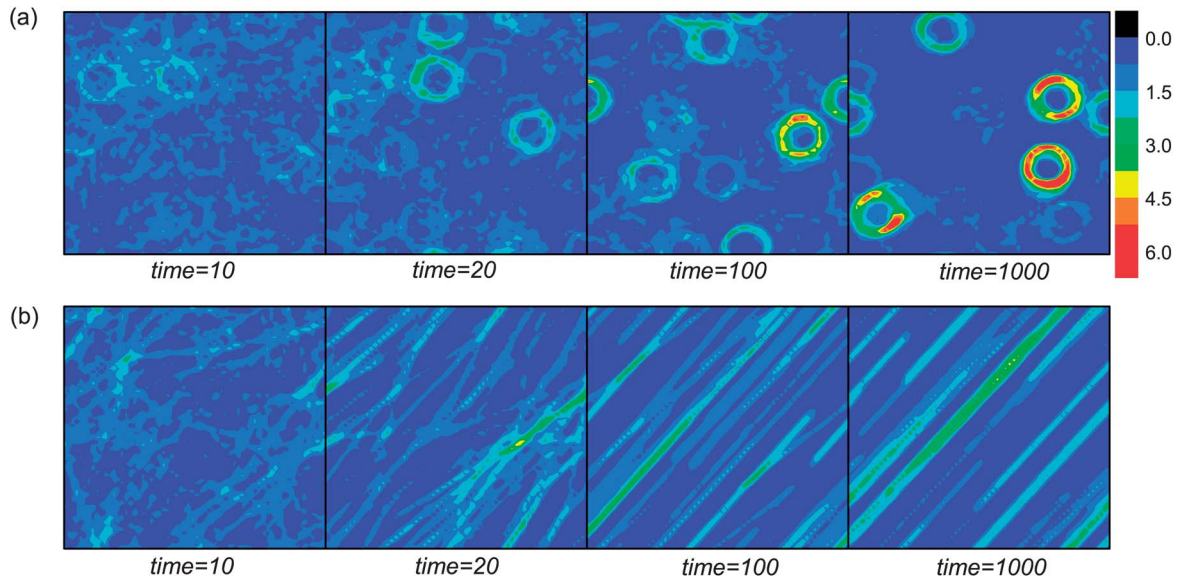

Fig. 5 Collective structures emerging from filaments with and without intra-filament HI interactions for $\alpha/10^3 = 6$, $\kappa/10^3 = 1.5$ and $L = 18$. Each image is averaged over the latest period of time $T = 10$. Parameters α, κ and L represent the active force, filament rigidity and filament length, respectively. Results with HI are shown in (a), while those without HI are shown in (b).

(b) indicates that rotation of a single filament is essential for the formation of collective vortexes. Thus, in a parameter region where intra-filament HI is important for the rotation of a single filament, it is also important for the emergence of vortexes. Collective structures of filaments with the same parameters except that the active forces are much larger ($\alpha/10^3 = 30$) are also studied. In this region, a single filament can rotate both with and without intra-filament HI. Similar vortexes to those shown in Fig. 5(a) are observed no matter HI is present or not, indicating that intra-filament HI is not necessary for the emergence of collective vortexes. In short, the finding that, intra-filament HI is important for the rotation of filament with small activation or large rigidity and not essential if activation is large or rigidity is small, provides a possible explanation at the single-filament level for the controversial points proposed in the beginning of the paper. Bending and activation, combined with local collisions, are sufficient for the collective vortexes formation in the parameter region where a single filament rotates, while the intra-filament HI helps vortexes to format in some parameter regions where a single filament does not rotate.

5 Conclusion

We have proposed a simple filament model involving both shape kinematics and intra-filament HI, and demonstrated that the instability and asymmetry of the shape kinematics can result in transitions between different types of filament motion (translation, snaking, and rotation). This study is motivated by the argument about the effect of HI on the formation of collective vortexes observed in experiments. As a first step, our findings provide insights into this issue by a detailed investigation of the motion of a single filament. A single filament can rotate spontaneously *via* a series of transitions from other types of motion no matter HI takes effect or not, and HI can enlarge remarkably the parameter region for filament rotation. With the same type of local collisions as in ref. 2, we show that if the active force is large (consequently, the parameter region for rotation is relatively large), intra-filament HI is not essential for the emergence of collective vortexes, which corresponds to the case studied in ref. 2. On the other hand, if the active force is small, the parameter region for rotation can be significantly enlarged when HI is considered. In this latter case, vortexes disappear if intra-filament HI effects are not taken into account, indicating that HI is important for the formation of collective vortexes. Thus, our work has made an important step toward the understanding of complex collective behaviors regarding active filaments. It also needs to be emphasized here that all the results we discussed mainly focus on dynamics with intra-filament interactions. As we know, the emergence of collective structures involves many other inter-filament interactions, *e.g.*, experiments showed that inter-filament HI is important for dynamics of filament clusters when they encounter with each other.[3] Thus, it is desirable to explore how inter-filament interactions (such as HI between filaments or clusters of filaments) affect the formation of collective structures. Extension of the proposed filament model to include inter-filament HI is straightforward, and we hope that our work can inspire more theoretical studies on the collective behaviors of active filaments.

Acknowledgements

This work is supported by the National Science Foundation of China (20933006, 91027012, 21125313) and National Basic Research Program of China (2013CB834606).

References

1 V. Schaller, C. Weber, C. Semmrich, E. Frey and A. R. Bausch, *Nature*, 2010, **467**, 73.
2 Y. Sumino, K. H. Nagai, Y. Shitaka, D. Tanaka, K. Yoshikawa, H. Chaté and K. Oiwa, *Nature*, 2012, **483**, 448.
3 V. Schaller, C. Weber, E. Frey and A. R. Bausch, *Soft Matter*, 2011, **7**, 3213.
4 P. Kraikivski, R. Lipowsky and J. Kierfeld, *Phys. Rev. Lett.*, 2006, **96**, 258103.
5 G. Jayaraman, S. Ramachandran, S. Ghose, A. Laskar, M. S. Bhamla, P. B. S. Kumar and R. Adhikari, *Phys. Rev. Lett.*, 2012, **109**, 158302.
6 J. Happel and H. Brenner, *Low Reynolds Number Hydrodynamics*, Prentice-Hall, 1965.
7 K. Sekinoto, N. Mori, K. Tawada and Y. Y. Toyoshima, *Phys. Rev. Lett.*, 1995, **75**, 172.
8 L. Bourdieu, T. Duke, M. B. Elowitz, D. A. Winkelmann, S. Leibler and A. Libchaber, *Phys. Rev. Lett.*, 1995, **75**, 176.
9 S. Camalet, F. Jülicher and J. Prost, *Phys. Rev. Lett.*, 1999, **82**, 1590.
10 S. Camalet and F. Jülicher, *New J. Phys.*, 2000, **2**, 24.
11 J. Elgeti, U. Kaupp and G. Gompper, *Biophys. J.*, 2010, **99**, 1018.
12 Y. Or, *Phys. Rev. Lett.*, 2012, **108**, 258101.
13 C.-C. Hsieh, L. Li and R. G. Larson, *J. Non-Newtonian Fluid Mech.*, 2003, **112**, 141.
14 J. P. Ryckaert, G. Ciccotti and H. J. C. Berendsen, *J. Comput. Phys.*, 1977, **23**, 327.
15 J. Rotne and S. Prager, *J. Chem. Phys.*, 1969, **50**, 4831.
16 H. Yamakawa, *J. Chem. Phys.*, 1970, **53**, 436.